NUMERICAL SIMULATION OF HORIZONTAL NONISOTHERMAL 3-D JET IN ROOM BY DSM

Shinsuke Kato, Shuzo Murakami, Ryozo Ooka
Institute of Industrial Science
University of Tokyo
Tokyo, Japan

SUMMARY

A three dimensional nonisothermal jet in a room is analyzed numerically by the standard $k-\varepsilon$ EVM (Eddy Viscosity Model) and two Second Moment Closure Models, i.e. Algebraic Stress Model (ASM) (Hossain and Rodi (1982)) and Differential Stress Model (DSM) (Launder, Reece and Rodi (1975)). Numerical results given by these turbulence models are compared with experimental ones and the prediction errors existing in the results are examined, thus clarifying the relative structural differences between $k-\varepsilon$ EVM and two Second Moment Closure Models. Since the Second Moment Closure Models clearly manifest the turbulence structures of the flowfield, they are more accurate than $k-\varepsilon$ EVM. A small difference between DSM and ASM is also observed, one based on an inappropriate approximation for the convection and diffusion terms in the Reynolds stress transport equations in ASM.

NUMERICAL SIMULATION OF HORIZONTAL NONISOTHERMAL 3-D JET IN ROOM BY DSM

Shinsuke Kato, Shuzo Murakami, Ryozo Ooka
Institute of Industrial Science
University of Tokyo
Tokyo, Japan

1. Introduction

It is self − evident that accurate prediction of room airflow and temperature distribution is required for rational design of indoor air climate in a room. A great deal of effort has been devoted to advancing numerical prediction techniques for airflow in rooms. The standard $k-\varepsilon$ Eddy Viscosity Model ($k-\varepsilon$ EVM) [1] has made many contributions to simulating room airflow with a certain degree of accuracy [2]. However, since the $k-\varepsilon$ EVM is based on the concept of locally determined isotropic eddy viscosity assuming the simple gradient transport hypothesis, this model is not so efficient in flowfields where the Reynolds stresses ($-\overline{u_iu_j}$) and heat flux ($\overline{u_i\theta}$) are significantly anisotropic. Yet such flowfields which include recirculation, supply or exhaust openings or with buoyancy effect are often observed in a room.

On the other hand, Second Moment Closure models, which do not use the concept of eddy viscosity and gradient transport hypothesis, i.e. DSM [3] or ASM [4], do not suffer from the many problems which originate from the gradient transport model. The Algebraic Stress Model (ASM) [4] [5] [6], which is one of the Second Moment Closure models, has been proved to be a more accurate turbulence model than the $k-\varepsilon$ EVM [7] [8]. However, it is also pointed out that the approximation of convection and diffusion terms in the $\overline{u_iu_j}$ transport equation is inappropriate in a complex flowfield [9].

In this paper, a nonisothermal jet in an enclosed space is analyzed by the standard $k-\varepsilon$ EVM, ASM and DSM [3] [10], focusing particularly on the anisotropic property of the flowfield and on the convections and diffusions of second moment quantities in turbulent statistics like $\overline{u_iu_j}$ or $\overline{u_i\theta}$. The structural differences among the three turbulence models are then examined in detail.

2. Model flowfield

The configuration of the enclosed space or room model used here is shown in Fig. 1. A cold jet is discharged in the center of the left-hand wall. The right-hand wall, with an exhaust opening at each corner, is heated. The dimensions of the model are shown in Fig.1. The Archimedes number of the supply jet is 0.016.

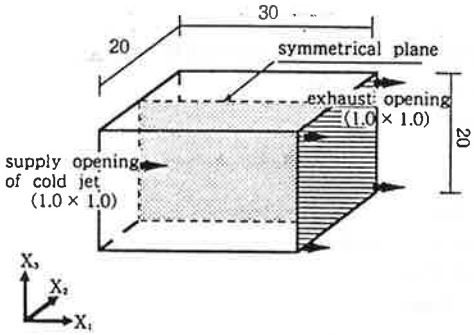

- Values are made dimensionless by L_o (one side of supply or exhaust opening), U_o (velocity at supply opening), $\Delta\Theta_o$ (temparature difference between exhaust and supply).
- In the experiment, U_o=1.0m/s, L_o=0.04m, $\Delta\Theta_c$=12.2 ℃. Consequently at the supply opening,

  Archimedes Number $A_r = \dfrac{-g_3 \cdot \beta \cdot \Delta\Theta_c \cdot L_o}{(U_o)^2} = 0.016$,

  and Reynolds number $R_e = 2.7 \times 10^3$.
  The scale of the enclosed space used for experiment : 1.2m(x_1) × 0.8m(x_2) × 0.8m(x_3).
- In the numerical simulation, it is assumed that $L_c = U_c = \Delta\Theta_c = 1.0$. Thus $A_r = -g_3 \cdot \beta$ and A_r is given the same value as in the experiment, 0.016.
  g_3 is defined to be negative in this paper.

Fig.1 Space Model for flowfield with buoyancy

Table 1 Basic Equations of Differential Stress Model

(Continuity Eq.) $\dfrac{\partial U_i}{\partial x_i} = 0$ (1)

(Momentum Eq.) $\dfrac{DU_i}{Dt} = -\dfrac{1}{\rho}\dfrac{\partial P}{\partial x_i} - \dfrac{\partial \overline{u_i u_j}}{\partial x_j} - g_i \beta \Theta$ (2)

($\overline{u_i u_j}$-Eq.) $\dfrac{D\overline{u_i u_j}}{Dt} = D_{ij} + P_{ij} + \Phi_{ij} + G_{ij} - \varepsilon_{ij}$ (3)

(ε-Eq.) $\dfrac{D\varepsilon}{Dt} = D_\varepsilon + \dfrac{\varepsilon}{k}(C_{\varepsilon 1}P_g + C_{\varepsilon 3}G_g - C_{\varepsilon 2}\varepsilon)$ (4)

(Θ-Eq.) $\dfrac{D\Theta}{Dt} = \dfrac{\partial}{\partial x_i}(-\overline{u_i\theta})$ (5)

($\overline{u_i\theta}$-Eq.) $\dfrac{D\overline{u_i\theta}}{Dt} = D_{i\theta} + P_{i\theta 1} + P_{i\theta 2} + \Phi_{i\theta} + G_{i\theta}$ (6)

($\overline{\theta^2}$-Eq.) $\dfrac{D\overline{\theta^2}}{Dt} = D_{\theta\theta} + P_{\theta\theta} - 2\cdot\varepsilon_\theta$ (7)

$k = \dfrac{1}{2}\overline{u_i u_i}$ (8) $P_k = \dfrac{1}{2}P_{ii}$ (9)

$G_k = \dfrac{1}{2}G_{ii}$ (10) $D_{ij} = \dfrac{\partial}{\partial x_m}(C_s \overline{u_m u_n}\dfrac{\partial}{\partial x_n}\overline{u_i u_j})$ (11)

$D_k = \dfrac{\partial}{\partial x_m}(C_s \overline{u_m u_n}\dfrac{\partial k}{\partial x_n})$ (12) $D_{i\theta} = \dfrac{\partial}{\partial x_m}(C_{s\theta}\overline{u_m u_n}\dfrac{\partial}{\partial x_n}\overline{u_i\theta})$ (13)

$D_\varepsilon = \dfrac{\partial}{\partial x_m}(C_{s\varepsilon}\overline{u_m u_n}\dfrac{\partial \varepsilon}{\partial x_n})$ (14) $P_{ij} = -\overline{u_i u_n}\dfrac{\partial U_j}{\partial x_n} - \overline{u_j u_n}\dfrac{\partial U_i}{\partial x_n}$ (15)

$P_{i\theta 1} = -\overline{u_i u_n}\dfrac{\partial \Theta}{\partial x_n}$ (16) $P_{i\theta 2} = -\overline{u_i\theta}\dfrac{\partial U_i}{\partial x_n}$ (17)

$P_\varepsilon = -2\cdot\overline{u_i\theta}\dfrac{\partial \Theta}{\partial x_i}$ (18) $G_{i\theta} = -\overline{u_i\theta}\cdot g_1\cdot\beta - \overline{u_2\theta}\cdot g_1\cdot\beta$ (19)

$G_{ii} = -g_i\cdot\beta\cdot\overline{\theta^2}$ (20) $\varepsilon_{ij} = \dfrac{2}{3}\cdot\delta_{ij}\varepsilon$ (21)

$\Phi_{ij} = \Phi_{ij1} + \Phi_{ij2} + \Phi_{ij3} + \Phi^w_{ij1} + \Phi^w_{ij2}$ (22)

$\Phi_{ij1} = -C_1\dfrac{\varepsilon}{k}(\overline{u_i u_j} - \dfrac{2}{3}\delta_{ij}\varepsilon)$ (23) $\Phi_{ij2} = -C_2(P_{ij} - \dfrac{2}{3}\delta_{ij}P_{ii})$ (24)

$\Phi_{ij3} = -C_3(G_{ij} - \dfrac{2}{3}\delta_{ij}G_{ii})$ (25)

$\Phi^w_{ij1} = \sum_{n=1}^{N} C_1\dfrac{\varepsilon}{k}(\overline{u_k u_m}\cdot n_k^{(w)}\cdot n_m^{(w)}\cdot\delta_{ij} - \dfrac{3}{2}\overline{u_i u_j}\cdot n_i^{(w)}\cdot n_j^{(w)}$
$- \dfrac{3}{2}\overline{u_i u_j}\cdot n_i^{(w)}\cdot n_j^{(w)})\cdot\dfrac{k^{3/2}}{C_s\cdot h_n^{(w)}\varepsilon}$ (26)

$\Phi^w_{ij2} = \sum_{n=1}^{N} C_2(\Phi_{mk3}\cdot n_k^{(w)}\cdot n_m^{(w)}\cdot\delta_{ij} - \dfrac{3}{2}\Phi_{ik3}\cdot n_k^{(w)}\cdot n_j^{(w)}$
$- \dfrac{3}{2}\Phi_{jk3}\cdot n_k^{(w)}\cdot n_i^{(w)})\cdot\dfrac{k^{3/2}}{C_s\cdot h_n^{(w)}\varepsilon}$ (27)

$\Phi_{i\theta} = \Phi_{i\theta 1} + \Phi_{i\theta 2} + \Phi^w_{i\theta 1}$ (28)

$\Phi_{i\theta 1} = -C_{\theta 1}\dfrac{\varepsilon}{k}\cdot\overline{u_i\theta}$ (29) $\Phi_{i\theta 2} = -C_{\theta 2}P_{i\theta 2}$ (30)

$\Phi_{i\theta 3} = -C_{\theta 3}G_{i\theta}$ (31)

$\Phi^w_{i\theta 1} = \sum_{n=1}^{N} C_{\theta 1}\dfrac{\varepsilon}{k}\cdot\overline{u_i\theta}\cdot n_k^{(w)}\cdot n_i^{(w)}\cdot\dfrac{k^{3/2}}{C_s\cdot h_n\varepsilon}$ (32)

$\varepsilon_\theta = \dfrac{1}{2R}\dfrac{\overline{\theta^2}}{k}\varepsilon$ (33)

Table 2 Numerical Constants in Second Moment Closure Model

C_1 : 1.8 C_2 : 0.6 C_3 : 0.6 C_1' : 0.5 C_2' : 0.0 C_s : 0.22 C_ε : 0.16 $C_{\varepsilon 1}$: 1.44 $C_{\varepsilon 2}$: 1.92
$C_{\varepsilon 3}$: 1.44 (when $G_k > 0$) 0.0 (when $G_k \leq 0$) $C_{s\theta}$: 0.15 $C_{\theta 1}$: 3.0 $C_{\theta 2}$: 0.5 $C_{\theta 3}$: 0.3
$C_{\theta 1}'$: 0.5 R : 0.8 C_θ : 0.15 C_w : 2.5

3. Outline of numerical method

The commonly adopted formulation for DSM [3] [8] utilizes the equations shown in Table 1 (cf. Appendix 1 and 2). The formulation for ASM uses approximations for the convection and diffusion terms in $\overline{u_i u_j}$-equation (Eq.(3)) and $\overline{u_i\theta}$-equation (Eq. (8)) in the formulation of DSM (cf. appendix 3). Density fluctuation is neglected except in the buoyancy term (Boussinesq approximation).

The contribution of the generation by buoyancy effect to the transport equation of

Nomenclature

U_i = average velocity component in i direction
u_i = fluctuating velocity component in i direction
U_0 = velocity at supply opening
L_0 = length of one side of supply or exhaust opening
$-\overline{u_iu_j}$ = Reynolds stress component
P = average pressure
C_{ij} = convection term of $\overline{u_iu_j}$
D_{ij} = diffusion term of $\overline{u_iu_j}$
P_{ij} = generation rate of $\overline{u_iu_j}$ due to velocity gradient
G_{ij} = generation rate of $\overline{u_iu_j}$ due to bouyancy effect
ε_{ij} = dissipation rate of $\overline{u_iu_j}$
Φ_{ij} = pressure – strain correlation term
k = turbulent kinetic energy
C_k = convection term of k
P_k = generation rate of k due to velocity gradient
D_k = diffusion term of k
G_k = generation rate of k due to bouyancy effect
ε = dissipation rate of k
Θ = average value of temperature
θ = fluctuation of temperature
$\Delta\Theta_0$ = temperature difference between exhaust and supply
g_i = gravitational acceleration in i direction
$\overline{u_i\theta}$ = turbulent heat flux in i direction
$C_{i\theta}$ = convection term of $\overline{u_i\theta}$
$D_{i\theta}$ = diffusion term of $\overline{u_i\theta}$
$P_{i\theta}$ = generation rate of $\overline{u_i\theta}$
$G_{i\theta}$ = generation rate of $\overline{u_i\theta}$ due to buoyancy effect
$\Phi_{i\theta}$ = correlation term of pressure and scalar gradient
$\overline{\theta^2}$ = mean square of scalar fluctuation
C_{θ^2} = convection term of $\overline{\theta^2}$
D_{θ^2} = diffusion term of $\overline{\theta^2}$
P_{θ^2} = generation rate of $\overline{\theta^2}$
ε_θ = dissipation rate of $\overline{\theta^2}/2$
A_r = Archimedes Number ($\equiv -g_j\cdot\beta\cdot\Delta\Theta_r\cdot L_0/(U_0)^2$)
R_e = Reynolds number at supply opening($\equiv U_0\cdot L_0/\nu$)
$h_w^{(w)}$ = vertical distance from the w – th wall
σ_k = turbulent Prandtl number for k
σ_θ = turbulent Prandtl number for Θ
R = time scale ratio $((\overline{\theta^2}/2)/\varepsilon_\theta)/(k/\varepsilon)$
ν_t = eddy viscosity

Superscripts

$\cdot\ \overline{\ \ }\ \cdot$ = averaging operation
"wo" = total number of boundaries which enclose each region
"(w)" = the w – th wall

Subscripts

i, j, k = spatial coordinate indices
1 : streamwise direction (jet discharging direction)
2 : lateral direction
3 : vertical direction.

Values are made dimensionless by L_0, U_0 and $\Delta\Theta_0$. (cf. Appendix 1)

Table 3 Boundary Conditions (expressed by dimensionless value)

(Boundary at supply opening) $U_{IN} = 1.0$ $\overline{u_iu_i} = 0.0012$ $\ell = 0.325$ $\Theta_{IN} = 0.0$ $\overline{u_iu_j} = 0.0$

(Boundary at exhaust opening) $U_{OUT} = 0.25$ $\overline{u_iu_i}$, ε, Θ : free slip condition $\overline{u_iu_j} = 0.0$

(Wall boundary) The wall shear stress τ_w is given by equation①, following Launder and Spalding (1974).

Velocity gradient at the wall is given by equation②, which is used to calculate the generation term at the near – wall node. The value of ε at the near – wall node used for the transport equation for normal stress is expressed by equation ③ as a form averaged in a control – volume and defined as $\overline{\varepsilon}$. The value of normal stress at the wall is given by free slip condition. The value of ε at the near – wall node used for the transport equation of ε is defined by equation④.

$$\frac{U_i}{(\tau_w/\rho)}(C_\mu^{1/4}\cdot k)^{1/2}=\frac{1}{\kappa}ln\left[\frac{E\cdot(h_i/2)\cdot(C_\mu^{1/4}\cdot k)^{1/2}}{\nu}\right] \quad ① \qquad \left\{(\nu+\nu_t)\frac{\partial U}{\partial y}\right\}\Big|_{w+\Delta L}=\tau_w/\rho \quad ②$$

$$\bar{\varepsilon}=\frac{C_\mu^{3/4}k^{3/2}}{\kappa(h_i/2)}ln\left[\frac{E\cdot(h_i/2)\cdot(C_\mu^{1/4}\cdot k)^{1/2}}{\nu}\right] \quad ③ \qquad \varepsilon_1=\frac{C_\mu^{3/4}k^{3/2}}{\kappa(h_i/2)} \quad ④$$

Heat flux at heated wall : $\overline{u_i\theta} = -0.0025$. Heat flux at other walls $\overline{u_i\theta} = 0.0$.

$\kappa = 0.4$, $C_\mu = 0.09$, $E = 9.0$, $\nu = 1/R_e = 1/(2.7\times10^4)$, $\nu_t = C_\mu k^2/\varepsilon$

Table 4 Grids and Schemes for calculation

The computational domain is discretized as $35(x_1)\times22(x_2)\times54(x_3)$.

One side of the supply and exhaust openings is divided into 4 grids. Minimum grid size is 0.25 and maximum is 1.0.

One-half the space in the x_3 direction is calculated, considering the symmetrical property of the flowfield.

The convection term of all quantities is calculated by means of the QUICK scheme, except for the area just around the supply and exhaust openings, where the first – order upwind scheme is used.

The generation of $\overline{u_i\theta}$ due to $\overline{\theta^2}$ was not considered, because this generation was estimated through preliminary analysis to be much smaller than the generation due to velocity gradient or temperature gradient. Consequently, calculations for $\overline{\theta^2}$ and ε_θ are not made.

ε (Eq.4) is taken into account, following the method proposed by Viollet (1986) [11] (see Appendix 4). The standard $k-\varepsilon$ EVM is shown in Appendix 5.

Table 2 shows the various numerical constants used in the model, which follow those proposed by Launder, Reece, Rodi (1975) [3] and Launder (1983) [10]. The boundary conditions are shown in Table 3. Table 4 denotes grids and schemes for calculation.

In order to stabilize the numerical integration of momentum and temperature transport equations (Eqs.(2) and (5)), we have introduced the pseud viscosity method proposed by Huang and Leschziner (1985) [12] (Appendix 6).

A wall boundary using wall function is adopted, following Launder and Spalding (1974) [1]. At the heated wall on the right-hand side, the value of the heat flux is given as a boundary condition.

Grid discretization is 35 (x_1) × 22 (x_2) × 54 (x_3). Here x_1 denotes the horizontal direction of jet discharge and x_3 means the vertical direction. One-half of the space in the x_2 direction is analyzed, considering the symmetrical property of the flowfield.

A staggered grid system is adopted. For the transport equations of all quantities, a second-order upwind scheme (the QUICK scheme) is applied for the convection terms. The Adams-Bashforth scheme is used for time marching. The numerical integration is conducted following the ABMAC method (simultaneous iteration method for pressure and velocity).

4. Outline of model experiment

The scale of the model used in the experiment is 1.2m (x_1) × 0.8m (x_2) × 0.8m (x_3), as shown in Fig.1. The outside of the model is thermally insulated.

The accurate measurement of air velocity in a 3-D nonisothermal flowfield is very difficult. Average velocity is measured with a thermistor anemometer in this experiment. A 3-D ultrasonic anemometer of 5cm span is utilized for fluctuating velocity. One shortcoming of the latter anemometer is the wideness of the averaging length (5cm), thus the values of $\overline{u_i u_j}$, k etc. are given as the average for 5cm. Therefore the measuring space-intervals of those quantities are of necessity much larger than those of average velocity or temperature, as shown in Figs. 4, 5 and 6.

Temperature is measured by C_o-C_u thermocouples. The heat generation rate at the right-hand heating wall is measured by an electronic power meter.

5. Results and discussion

5.1 Distribution of mean velocity U_i (Figs. 2, 5)

The distributions of scalar velocity ($\sqrt{U_1^2+U_2^2+U_3^2}$) and velocity vector at the central vertical section are illustrated in Figs. 2 and 5.

Above the centerline of the jet, the vertical temperature gradient is positive and the flow is rather stable. Below the centerline, the temperature gradient is negative and the flow is unstable to some degree. From this point of view, the velocity value in the area around the center of the jet is very important. In this area the values given by $k-\varepsilon$ EVM are generally larger than those given by the other Second Moment Closure models. This tendency corresponds to the smaller values of Reynolds stress

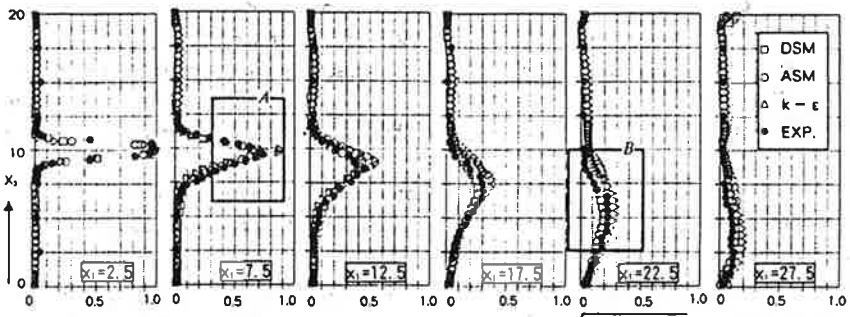

Figure 2 Comparison of scalar velocity distribution $U = \sqrt{U_1^2 + U_2^2 + U_3^2}$ *(dimensionless value by* U_0*, at center section).*

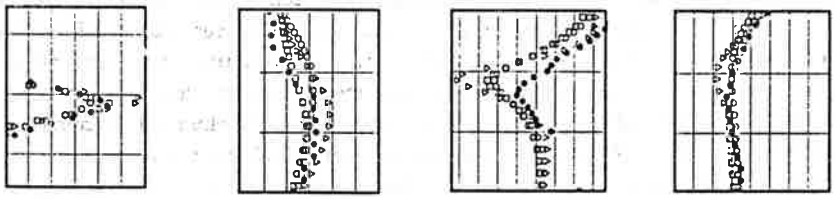

Fig. 2. A *Fig. 2. B* *Fig. 3. C* *Fig. 3. D*

Figures magnified at $x_1 = 12.5, 22.5$ *for Fig. 2 and* $x_1 = 7.5, 17.5$ *for Fig. 3*

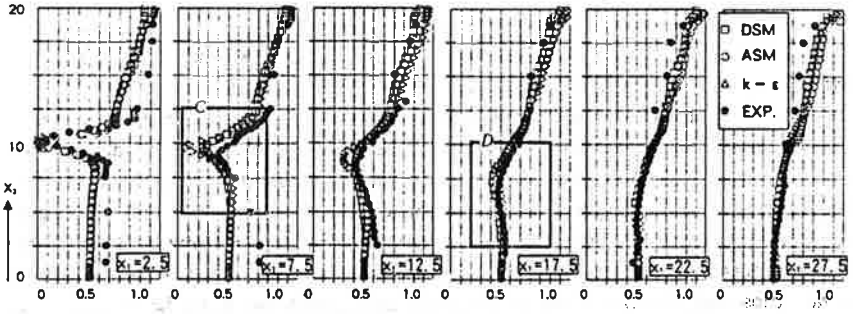

Figure 3 Comparison of temperature distribution Θ *(dimentionless value by* $\Delta\Theta_0$*, at center section)*

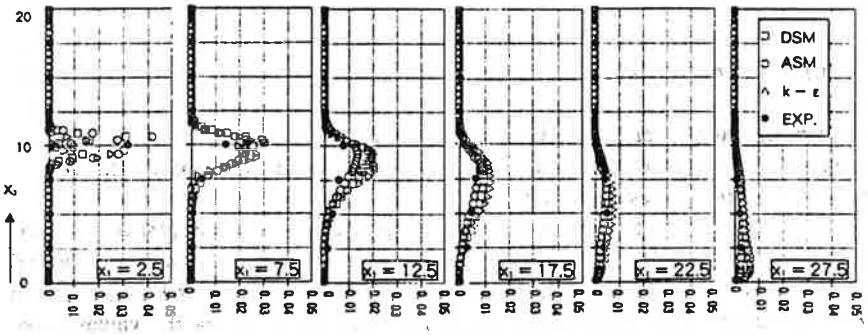

Figure 4 Comparison of turbulent energy k

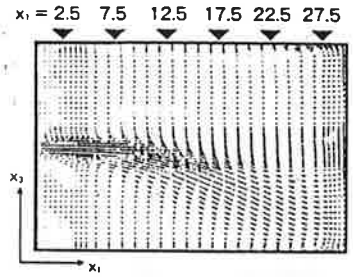

Figure 5 Distribution of velocity vectors (result of DSM at center section). supply velocity ——→

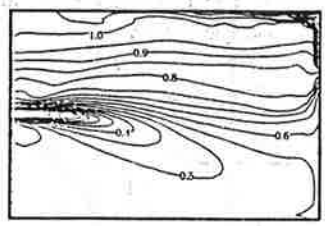

Figure 6 Distribution of temperature Θ (result of DSM at center section)

given by $k-\varepsilon$ EVM in comparison with those given by ASM and DSM. This inadequate lower level of the Reynolds stress implies insufficient diffusion of the mean momentum, which gives rise to larger mean velocities at the centerline. In the area just after the jet discharge, the values given by DSM are a little higher than those given by ASM. However in the downstream region, the centerline speed of the cold jet given by DSM has lower values than does ASM. The position of the peak speed observed in DSM is located lower in the x_3 direction than in ASM, that is, the jet predicted by DSM drops faster than does that predicted by ASM. The agreement between DSM and the experiment is the best among the three models. This is attributable to the fact that the evaluation of $\overline{u_iu_j}$ in the momentum equation given by DSM is more accurate than those given by the two other models. A comparison of $\overline{u_iu_j}$ of these models is described below in § 5.5.

5.2 Distribution of mean temperature Θ (Figs.3, 6)

The temperature distributions at the area around the center of the jet are also very important. Except for the area just after the jet discharge, the distributions given by both ASM and DSM generally show less steep gradients than those given by $k-\varepsilon$ EVM. This tendency is caused by the difference in the evaluation of the turbulent heat flux $\overline{u_i\theta}$. Since ASM and DSM predict larger values of $\overline{u_i\theta}$ than does $k-\varepsilon$ EVM (Fig.11), the diffusion of the temperature difference around the center of the jet in the case of ASM and DSM is more active than that given by $k-\varepsilon$ EVM.

There is little difference between ASM and DSM. However, if we are forced to compare them, the distribution given by DSM shows a slightly steeper gradient in this area. This derives from the fact that the absolute value of $\overline{u_i\theta}$ given by DSM is lower than that given by ASM at the upstream area of the jet (Fig.11). However, the results of DSM show slightly poorer agreement with the experiment here than does ASM. Generally, the results of all three models show poor agreement with the experimental results in the areas below and above the jet just after the discharge. Some comments concerning these poor agreements are given in Appendix 7.

5.3 Distribution of turbulent energy k (Fig.4)

In the area just after the jet discharge, where all three turbulence models predict steep gradients of velocity and temperature, the predicted values of k given by ASM and DSM are larger than those given by $k-\varepsilon$ EVM. However, in the downstream region of the jet, the values of the two Second Moment Closure models are to the contrary smaller than those of $k-\varepsilon$ EVM. This is due to the fact that the Second

Moment Closure models predict Reynolds stress ($\overline{u_iu_j}$) more accurately, since they are not based on isotropic eddy viscosity and consequently predict the value of kinetic energy generation by mean shear P_k more accurately than does $k-\varepsilon$ EVM. The values predicted by DSM generally tend to be a little larger than the experimental data. Some comments concerning this difference are given in Appendix 8.

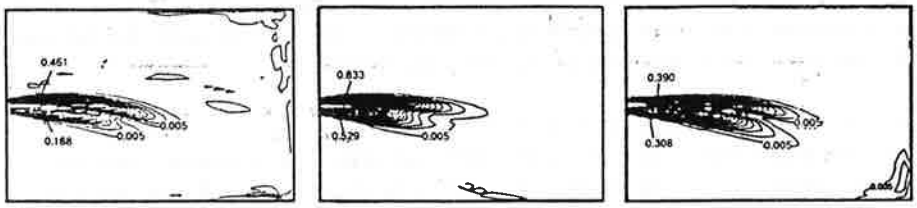

(1) DSM (2) ASM (3) $k-\varepsilon$ EVM

Figure 7 Comparison of generation term of k (P_k)

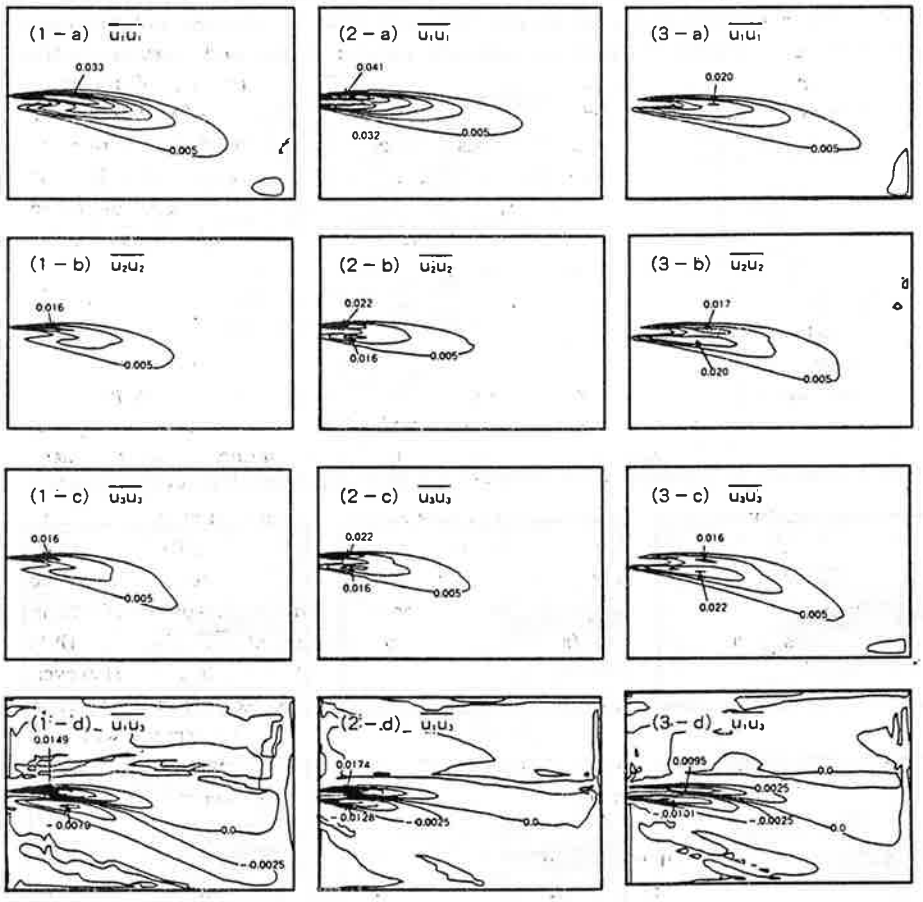

(1) DSM (2) ASM (3) $k-\varepsilon$ EVM

Figure 8 Comparison of Reynolds stress $\overline{u_iu_j}$

5.4 Distribution of P_k (Fig.7)

The values of P_k given by the two Second Moment Closure models become larger in the area near the supply opening and smaller in the downstream area compared with those given by $k-\varepsilon$ EVM. Comparing DSM and ASM, the value of P_k given by DSM is a little smaller in the area near the supply opening and a little larger in the downward area. These differences are caused by the differences in $\overline{u_iu_j}$ between DSM and ASM, as is explained in the following section.

5.5 Distribution of Reynolds stress $\overline{u_iu_j}$ (Fig.8)

In the distributions given by both DSM and ASM, the anisotropic property of normal stresses $\overline{u_iu_i}$ is reproduced very well, as is shown in Fig 8. The value of $\overline{u_1u_1}$ becomes about two times larger than $\overline{u_2u_2}$ and $\overline{u_3u_3}$ in the case of the Second Moment Closure models, while $k-\varepsilon$ EVM fails to reproduce this anisotropic property. Fig. 9 illustrates the difference between the Second Moment Closure model and $k-\varepsilon$ EVM in the evaluation of $\overline{u_iu_j}$. Comparing DSM and ASM, the absolute values of each component of $\overline{u_iu_i}$ given by DSM are generally smaller in the area near the supply

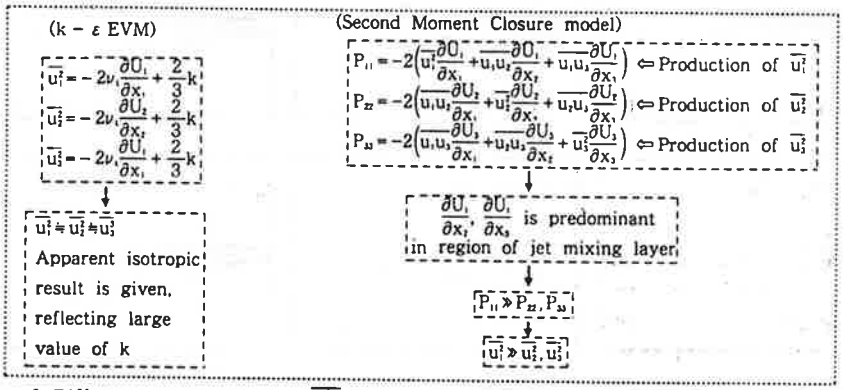

Figure 9 Difference of evaluation of $\overline{u_iu_j}$ between $k-\varepsilon$ EVM and Second Moment Closure model

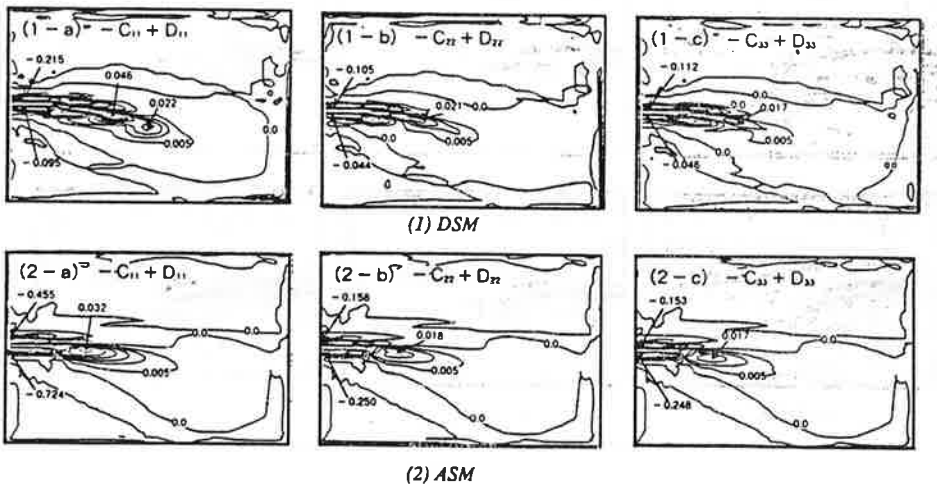

(1) DSM

(2) ASM

Figure 10 Comparison of convection and diffusion term in $\overline{u_iu_j}$- equation ; $-C_{ij}+D_{ij}$

opening and larger in the downstream area. This is attributable to the fact that DSM evaluates convection and diffusion terms in the $\overline{u_iu_j}$-equation more accurately than does ASM. In the modeling of ASM, it is assumed that the flowfield in concern is almost in the state of local equilibrium i.e. the convective and diffusive effect is small, so the convective and diffusive transport of the second moment quantities could be evaluated proportionally to that of turbulence energy which is equal to the imbalance between turbulence energy production and dissipation. Consequently, the distribution of $\overline{u_iu_j}$ given by ASM is determined mainly by the production and pressure-strain correlation terms (see Appendix 3, Eq.①). In this context, the distributions of $\overline{u_iu_j}$ in ASM are influenced too strongly by the evaluation of the production term. On the other hand, in the case of DSM, the distribution of $\overline{u_iu_j}$ has a larger value at the centerline of the jet in the downstream area compared with ASM because the $\overline{u_iu_j}$ generated just after the jet discharge is transported to the downstream region by the accurately predicted convective and diffusive terms. This is illustrated in Fig. 10 where the convection and diffusion terms in the $\overline{u_iu_j}$-equation predicted by the two Second Moment Closure models are shown. Obviously, DSM predicts the effect of convection and diffusion to be more active in the downstream area than does ASM. Therefore the amount of $\overline{u_iu_j}$ generated just after the jet discharge is transported further downward in the case of DSM.

5.6 Distribution of turbulent heat flux $\overline{u_i\theta}$ (Fig.11)

The difference of $\overline{u_i\theta}$ between the two Second Moment Closure models and $k-\varepsilon$ EVM is very large. In particular, the difference for streamwise heat flux $\overline{u_1\theta}$ is remarkable. The value of $\overline{u_1\theta}$ predicted by $k-\varepsilon$ EVM is much smaller than the results given by both DSM and ASM. Since $\overline{u_1\theta}$ is calculated with $-\nu/\sigma_\theta \cdot \partial\Theta/\partial x_1$ in the case of $k-\varepsilon$ EVM, and $\partial\Theta/\partial x_1$ is rather small in this flowfield, the predicted value of $\overline{u_1\theta}$ naturally becomes small. However, in the case of Second Moment Closure models, all terms of generation by temperature gradient $P_{1\theta(1)}$ and velocity gradient $P_{1\theta(2)}$ are evaluated exactly :

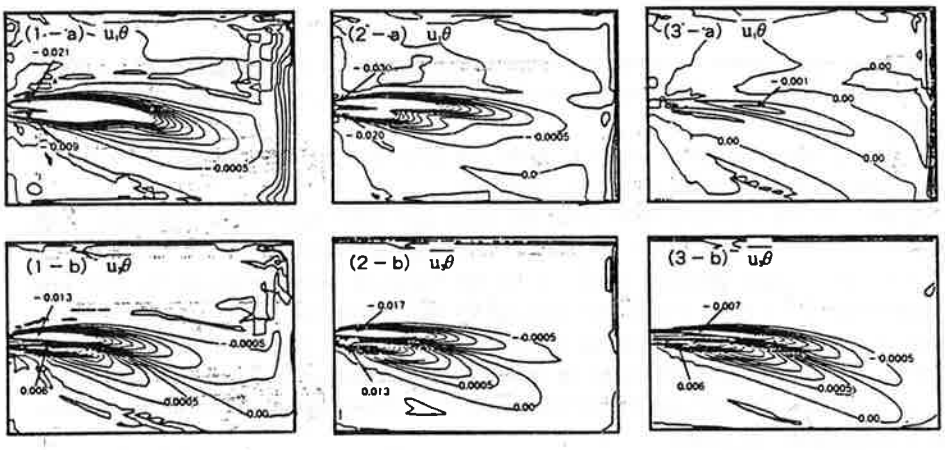

(1) DSM *(2) ASM* *(3) k − ε EVM*

Figure 11 Comparison of turbulent heat flux, $\overline{u_i\theta}$

$$P_{\theta(1)} = -\overline{u_1^2}\frac{\partial\Theta}{\partial x_1} - \overline{u_1u_2}\frac{\partial\Theta}{\partial x_2} - \overline{u_1u_3}\frac{\partial\Theta}{\partial x_3}, \tag{34}$$

$$P_{\theta(2)} = -\overline{u_1\theta}\frac{\partial U_1}{\partial x_1} - \overline{u_2\theta}\frac{\partial U_1}{\partial x_2} - \overline{u_3\theta}\frac{\partial U_1}{\partial x_3}. \tag{35}$$

Hence, the contribution of the predominant term of the temperature gradient $\partial\Theta/\partial x_3$ and the predominant term of the velocity gradient $\partial U_1/\partial x_3$ to the production of $\overline{u_1\theta}$ is reflected correctly. Thus the value of $\overline{u_1\theta}$ given by the second moment closure models becomes large. Comparing DSM and ASM in the same way as was done above in the analysis of $\overline{u_iu_j}$, the absolute values of each component of $\overline{u_i\theta}$ given by DSM are also smaller in the area near the supply opening and larger in the downstream area compared with those given by ASM, because the evaluation of the convection and diffusion process is more accurate in DSM than in ASM (cf. Appendix 3 Eq.③).

The convection and diffusion terms in the $\overline{u_i\theta}$-equation predicted by DSM and ASM are shown in Fig. 12. Here, DSM predicts the effect of convection and diffusion to be more active, in particular in the $\overline{u_1\theta}$ component in the downstream area of the jet, than does ASM.

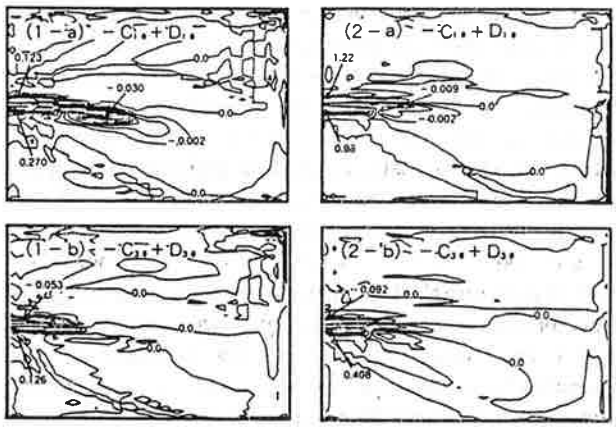

(1) DSM *(2) ASM*

Figure 12 Comparison of convection and difusion for $\overline{u_i\theta}$; $-C_{i,\theta} + D_{i,\theta}$

6. Conclusions

A three-dimensional anisotropic flowfield with buoyancy is analyzed by $k-\varepsilon$ EVM, ASM and DSM and the numerical results are then compared with the experimental ones.

①The predicted distribution of U_i given by DSM has the best agreement with the experiment among the three models used here.

②The numerical results of Θ given by DSM and ASM have better agreement with the experiment at the center of the jet than does $k-\varepsilon$ EVM.

③The anisotropic property of $\overline{u_iu_j}$ in the jet region is well reproduced by DSM and ASM, while $k-\varepsilon$ EVM reproduces nothing of this characteristic.

④The difference in $\overline{u_i\theta}$ predicted by the Second Moment Closure models and $k-\varepsilon$ EVM, in particular the difference in streamwise heat flux $\overline{u_1\theta}$, is remarkable, because $k-\varepsilon$ EVM does not include the contributions of the predominant terms of the velocity and temperature gradients.

⑤Values of second moment quantities, i. e. $\overline{u_iu_j}$, $\overline{u_i\theta}$, predicted by DSM have larger peak values in the downstream area compared with ASM.

Appendix 1

The equations in Table 1 are not expressed in dimensionless form. For example, the buoyancy term $(-g_i \cdot \beta \cdot \Theta)$ is expressed as $(Ar \cdot \Theta')$ by normalization. Here Θ' is the dimensionless temperature.

Appendix 2

$\Phi^w_{ij(2)}$ is not involved in this calculation. This is because the Gibson－Launder (1978) model of $\Phi^w_{ij(2)}$, which is most common at present, appears to have some shortcomings in the analysis of a flowfield with impinging [5]. The reason is as follows.

Let us imagine a situation of impinging in which a mean flow (U_1) attacks the opposite wall existing in a $x_2 - x_3$ perpendicular plane. In this situation, $\Phi^w_{ij(2)}$ may be represented in the following manner :

$$\Phi^w_{11(2)} = 2C_2C_2'(P_{11}-2/3P_k)\cdot f_1,$$

$$\Phi^w_{22(2)} = \Phi^w_{33(3)} = -C_2C_2'(P_{11}-2/3P_k)\cdot f_1.$$

Here

$$f_1 = k^{3/2}/(C_\ell \cdot \varepsilon \cdot h_1).$$

$\Phi^w_{ij(2)}$ is the term that should decrease $\overline{u_1^2}$ according to its original definition, since $\overline{u_1^2}$ is the normal perpendicular to a wall. Thus, in this case, $(P_{11}-2/3P_k)$ must be negative. However, on the centerline of the impinging jet, P_{11} is large. Therefore, it does not take a negative value. Hence, in this model, $\Phi^w_{ij(2)}$ works to increase $\overline{u_1^2}$, contrary to its original meaning. As a matter of fact, when $\Phi^w_{ij(2)}$ is involved in the calculations, the normal stress perpendicular to the wall becomes excessively large near the exhaust opening and the solution diverges.

Recently T. J. Craft and B. E. Launder have proposed a new model of $\Phi^w_{ij(2)}$, which is applicable to an impinging region [13] [14].

Appendix 3

In the formulation of ASM, the convection term C_{ij} and the diffusion term D_{ij} which include derivatives of $\overline{u_iu_j}$ and $\overline{u_i\theta}$ are expressed in a simplified way as shown in Eqs.① and ② following the method of Rodi (1976) [4] and Gibson and Launder (1976) [5].

$$C_{ij} - D_{ij} = \frac{u_iu_j}{k}(C_k - D_k), \quad ①$$

$$C_{i\theta} - D_{i\theta} = \frac{u_i\theta}{2}\left(\frac{1}{k}(C_k - D_k) + \frac{1}{\theta^2}(C_\theta - D_\theta)\right). \quad ②$$

As $\overline{\theta^2}$ is not calculated in this study, we use the following instead of ②

$$C_{i\theta} - D_{i\theta} = \frac{u_i\theta}{k}(C_k - D_k). \quad ③$$

Appendix 4

The ε equation is so revised that an expression of the buoyancy generation/destruction term is switched according to the locally determined thermal instability, following the method proposed by Viollet (1986), as follows. When $G_k > 0$, $C_3 = C_1 = 1.44$, and when $G_k \leq 0$, $C_3 = 0$

Appendix 5

The formulation for the standard $k-\varepsilon$ EVM is as follows :

$$\overline{u_iu_j} = -\nu_t\left(\frac{\partial U_i}{\partial x_j}+\frac{\partial U_j}{\partial x_i}\right)+\frac{2}{3}k, \quad ④$$

$$\overline{u_j\theta} = -\frac{\nu_t}{\sigma_\theta}\frac{\partial \Theta}{\partial x_j}, \quad ⑤$$

$$\frac{Dk}{Dt} = D_k+P_k+G_k-\varepsilon, \quad ⑥$$

$$\frac{D\varepsilon}{Dt} = D_\varepsilon+\frac{\varepsilon}{k}(C_{\varepsilon 1}P_k+C_{\varepsilon 3}G_k-C_{\varepsilon 2}\varepsilon), \quad ⑦$$

$$D_k = \frac{\partial}{\partial x_j}\frac{\nu_t}{\sigma_k}\frac{\partial k}{\partial x_j}, \quad ⑧$$

$$D_\varepsilon = \frac{\partial}{\partial x_j}\frac{\nu_t}{\sigma_\varepsilon}\frac{\partial \varepsilon}{\partial x_j}, \quad ⑨$$

$$\nu_t = C_\nu\frac{k^2}{\varepsilon}, \quad ⑩$$

σ_k: 1.0 σ_θ: 1.0 σ_ε: 1.3 C_ν: 0.09.

Appendix 6

A diffusion equation with convection can be expressed generally in the form :

$$\frac{\partial \phi}{\partial t}+U_j\frac{\partial \phi}{\partial x_j} = \alpha\frac{\partial^2\phi}{\partial x_j^2}, \quad ⓐ$$

where α means a positive diffusivity of ϕ and U_j is a convective velocity. This type of equation can be solved numerically without instability if we select an appropriate time step and an appropriate mesh system. However, the momentum equation in the DSM calculation is expressed as follows (Eq.(2)),

$$\frac{\partial U_i}{\partial t}+U_j\frac{\partial U_i}{\partial x_j} = -\frac{\partial P}{\partial x_i}+\frac{\partial}{\partial x_j}(-\overline{u_iu_j}). \quad ⓑ$$

The turbulent diffusion term of this equation ($\partial(-\overline{u_iu_j})/\partial x_j$) is not expressed apparently as a form of a second derivative of U_i ,($\alpha\partial^2U_i/\partial x_j^2$), the gradient diffusion form. Therefore, Eq.ⓑ is not necessarily stable for the numerical integration.

The pseud viscosity method introduces the second derivative of U_i with positive coefficient into the turbulent diffusion term in Eq.ⓑ, using the mean velocity gradient involved in the production term of $\overline{u_iu_j}$-equation (Eq.(15)).

The $\overline{u_iu_j}$-equation in steady state can be written as follows

$$C_{ij}-D_{ij} = P_{ij}+\Phi_{ij}-\varepsilon_{ij}. \quad ⓒ$$

In the terms C_{ij} , D_{ij} and Φ_{ij} , $\overline{u_iu_j}$ is included, defined at the center of a calculating control volume (cell). Here, we decompose these terms as shown in Eq.ⓓ so that each coefficient such as A_c becomes positive.

$$C_{ij} = C_{ij}^* + A_c\cdot\overline{u_iu_j}, \quad D_{ij} = D_{ij}^* - A_D\cdot\overline{u_iu_j}, \quad \Phi_{ij} = \Phi_{ij}^* - A_*\cdot\overline{u_iu_j}, \quad ⓓ$$

where $*$ denotes the remainder of each term.

With Eq.ⓓ, Eq.ⓒ becomes

$$(A_c+A_D+A_*)\overline{u_iu_j} = P_{ij}+\Phi_{ij}^*+D_{ij}^*-C_{ij}^*-\varepsilon_{ij}. \quad ⓔ$$

Consequently, $\overline{u_iu_j}$ can be written in the form :

$$\overline{u_iu_j} = \frac{1}{A_c+A_D+A_*}(P_{ij}+\Phi_{ij}^*+D_{ij}^*-C_{ij}^*-\varepsilon_{ij}). \quad ⓕ$$

Since P_{ij} involves the mean velocity gradient ($\partial U_i/\partial x_j$) as shown in Eq.(15) (only selecting $k=j$ component in $-\overline{u_iu_k}\partial U_j/\partial x_k$), Eq.ⓕ can be rewritten as follows, where the velocity gradient ($\partial U_j/\partial x_i$) in P_{ij} is separated from the other terms.

$$\overline{u_iu_j} = \frac{1}{A_c+A_D+A_*}\left(-\overline{u_iu_j}\frac{\partial U_i}{\partial x_j}+Se\right), \quad ⓖ$$

where we have no summation in $-\overline{u_iu_j}\partial U_j/\partial x_j$ for suffix j and Se means the remainders . Substituting Eq.ⓖ into Eq.ⓑ, it becomes

$$\frac{\partial U_i}{\partial t}+U_j\frac{\partial U_i}{\partial x_j} = -\frac{\partial P}{\partial x_i}+\frac{\partial}{\partial x_j}\left(\frac{\overline{u_iu_j}}{A_c+A_D+A_*}\frac{\partial U_i}{\partial x_j}-\frac{Se}{A_c+A_D+A_*}\right), \quad ⓗ$$

where the coefficient in the second derivative of U_i in the diffusion term, $\overline{u_iu_j}/(A_*+A_D+A_c)$ is always positive because normal stress $\overline{u_iu_j}$ is always positive. This coefficient is called pseud viscosity. The term $Se/(A_*+A_D+A_c)$ is treated in the same

manner with source term. This formulation is similar to the diffusion equation ⓐ. Hence we can expect numerical stability in the calculation of Eq.ⓑ which does not include the second derivative with a positive coefficient ($a\partial^2 U_i/\partial x_j^2$) in its original form.

Appendix 7

Since the jet is discharged into stagnant air, the air velocity is almost zero in the area above and below the jet just after discharge, as shown in Figures 2 and 4. The agreement between the experiment and the numerical simulation for the temperature distribution is poor in this area. The reason for the disagreement may be explained as follows :

1. Since the air velocity is very low in such areas, the slow secondary flows caused by disturbances to the experimental conditions become rather effective, giving rise to uncertainty in the experimental results. The realization of a strictly controlled experimental condition is very difficult for such types of flow and temperature fields.

2. Although the turbulence models are based on the assumption that the flow field is fully turbulent, the Reynolds number in this area is rather low and not fully turbulent.

3. There is some possibility that the simulation has not yet reached a sufficiently steady state.

Appendix 8

The average length of the anemometer is rather large (5cm) and the values of k are averaged within this length in the experiment. Here there is some possibility that it fails to pick up small fluctuations. This might be one reason why the value predicted by DSM is generally larger than the experimental data.

REFERENCES

[1] Launder, B.E., and D.B. Spalding. 1974. The numerical computation of turbulent flow. *Computer Methods in Applied Mechanics and Engineering* 3 : 269 – 289.

[2] Murakami, S., S. Kato, and H. Nakagawa. 1991. Numerical prediction of horizontal nonisothermal 3 – D jet in room based on the k – ε model. *ASHRAE Transactions* 97 (1) : 38 – 48.

[3] Launder, B.E., G.J. Reece, and W. Rodi 1975. Progress in the development of a Reynolds stress turbulence closure. *J. Fluid Mech.* 68 : 537 – 566.

[4] Rodi. W. 1976. A new algebraic relation for calculating the Reynolds stress. *ZAMM* (56) : T219 – T221.

[5] Gibson, M.M. and B.E. Launder 1976. On the calculation of horizontal turbulent free shear flows under gravitational influence *J. Heat Transfer*, 2 81 – 87.

[6] Hossain, M.S., and W. Rodi. 1982. A turbulence model for buoyant flows and its application to vertical buoyant jets. *In Turbulent Buoyant Jets and Plumes*, W.Rodi, ed., HMT – Series, Vol.6. Oxford, UK : Pergamon Press.

[7] Murakami, S., S. Kato, and Y. Kondo 1991. Examining k – ε EVM by means of ASM for a 3 – D horizontal buoyant jet in enclosed space *Engineering Turbulence Modelling and Experiments* Rodi and Ganic, ed., Elsevier Science Publishing., 205 – 214.

[8] Murakami, S., S. Kato, and Y. Kondo 1992. Numerical prediction of Horizontal nonisothermal 3 – D jet in room based on Algebraic Second – Moment Closure Model.

ASHRAE Transactions 98 (1).

[9] Murakami, S., A. Mochida, Y. Hayashi, 1991. Scrutinizing k-ε EVM and ASM by means of LES and wind tunnel for flowfield around cube. *Proc. 8th Symposium on turbulent shear flows.* 17, 1. 1 – 17. 1. 6.

[10] Launder, B.E. 1983. Second – moment closure, methodology and practice. *Univ. Manchester Institute Sci and Tech., Rep.* TFD/82/4.

[11] Viollet, P.L, 1986. On the numerical modeling of the stratified flows. *Proc. Symposium Physical Processes in Estuarie.*

[12] Haung, P.G., and M.A. Leschziner 1985. Stabilization of recirculating flow computations performed with second – moment closures and third – order discretization. *Proc. 5th Symposium on turbulent shear flows.* 20. 7 – 20. 12.

[13] Craft, T. J. and B.E. Launder 1991. Computation of impinging flows using second – moment closures, *Proc. 8th Symposium on turbulent shear flows.* 8. 5. 1 – 8. 5. 6.

[14] Craft, T. J. and B.E. Launder 1991. A New Model of 'Wall – Reflection' Effects on the Pressure – Strain Correlation and its Application to the Turbulent Impinging Jet. *AIAA Journal November.*